*American Mineralogist, Volume 85, pages 1275–1286, 2000*

# Crystal chemical variations in Li- and Fe-rich micas from Pikes Peak batholith (central Colorado)

**MARIA FRANCA BRIGATTI,*,[1] CRISTINA LUGLI,[1] LUCIANO POPPI,[1] EUGENE E. FOORD,† AND DANIEL E. KILE[2]**

[1]Department of Earth Sciences, University of Modena and Reggio Emilia, 41100 Modena, Italy
[2]United States Geological Survey, Denver, Colorado 80225, U.S.A.

## ABSTRACT

The crystal structure and M-site populations of a series of micas-1*M* from miarolitic pegmatites that formed within host granitic rocks of the Precambrian, anorogenic Pikes Peak batholith, central Colorado, were determined by single-crystal X-ray diffraction data. Crystals fall in the polylithionite-siderophyllite-annite field, being $0 \le Li \le 2.82$, $0.90 \le Fe_{total} \le 5.00$, $0.26 \le {}^{[6]}Al \le 2.23$ apfu. Ordering of trivalent cations (mainly $Al^{3+}$) is revealed in a cis-octahedral site (M2 or M3), which leads to a lowering of the layer symmetry from *C*12/*m*(1) (siderophyllite and annite crystals) to *C*12(1) diperiodic group (lithian siderophyllite and ferroan polylithionite crystals). On the basis of mean bond length, the ordering scheme of octahedral cations is mostly meso-octahedral, whereas the mean electron count at each M site suggests both meso- and hetero-octahedral ordering, the calculated mean atomic numbers being M1 = M3 ≠ M2, M2 = M3 ≠ M1 and M1 ≠ M2 ≠ M3. As the siderophyllite content increases, so do the *a*, *b,* and c unit-cell parameters, as well as the refractive indices, primarily $n_\beta$. The tetrahedral rotation angle, $\alpha$, is generally small ($1.51 \le \alpha \le 5.04°$) and roughly increases with polylithionite content, whereas the basal oxygen out-of-plane tilting, $\Delta z$, is sensitive both to octahedral composition and degree of order ($0.0 \le \Delta z \le 0.009$ Å for siderophyllite and annite, $0.058 \le \Delta z \le 0.144$ Å for lithian siderophyllite and ferroan polylithionite crystals).

## INTRODUCTION

This study concerns the crystal chemistry of trioctahedral micas from pegmatites associated with granitic units of the anorogenic Pikes Peak batholith (PPB), central Colorado. The PPB is a result of a complex magmatic history of crystallization and crustal assimilation, beginning with a mantle-derived basaltic magma and culminating with the miarolitic cavity stage of pegmatite evolution that represents the final product of crystallization (Simmons et al. 1987; Wobus and Hutchinson 1988; Černý, 1991; Foord et al. 1995; Kile and Foord 1998). Micas widely vary in composition, from annite in the host granite through siderophyllite and ferroan phlogopite in graphic pegmatites, and finally to lithian siderophyllite and ferroan polylithionite in miarolitic cavities (Foord et al. 1995; Kile and Foord 1998). In miarolitic pegmatites, micas, which are frequently Li- and Fe-enriched, have been used as markers of chemical fractionation and as petrogenetic indicators, as well as for characterizing relative HF, HCl, $O_2$, and $H_2O$ fugacities in fluids (Foord et al. 1995; Kile and Foord 1998). Therefore, the knowledge of crystal structure and chemistry, as well as of octahedral cation partitioning, can further our understanding of pegmatite evolution and conditions of crystallization.

The crystal structure of micas in the siderophyllite-polylithionite join was studied, for example, by Takeda et al. (1971), Sartori et al. (1973), Sartori (1976, 1977), Guggenheim and Bailey (1977), Brown (1978), Guggenheim (1981), Swanson and Bailey (1981), Backhaus (1983), Weiss et al. (1993), and Rieder et al. (1996). An interesting feature of these trioctahedral micas is the octahedral ordering pattern. The ideal layer symmetry reduces from *C*2/*m* to *C*2 space group, more precisely, referring to diperiodic groups, from *C*12/*m*(1) to *C*12(1) (Dornberger-Schiff et al. 1982), as the result of a different cation ordering in cis-octahedral sites.

Depending on the cation distribution of octahedral sites, Ďurovič (1994) subdivided micas in: (1) homo-octahedral (all three octahedral sites are occupied by the same kind of ions), (2) meso-octahedral (one site is occupied by a cation different from that in the other two sites), (3) hetero-octahedral (each of the three sites is differently occupied). The location of the origin of the octahedral sheet corresponds: (1) to the M1 site for homo-octahedral micas, (2) to the site with different occupation for meso-octahedral micas, and (3) to the site with the lowest electron density in hetero-octahedral micas (Ďurovič et al. 1984). Consequently, two kinds of layers exist (Zvyagin 1997; Nespolo et al. 1999): the M1 layer has an origin of the octahedral sheet in M1 site, whereas the M2 layer originates in either M2 or M3 site. The M1 layer is far more common. Meso-trioctahedral crystals along the trilithionite-polylithionite join, solved in the space group *C*2/*m* for 1*M* [Takeda and Burnham 1969, Guggenheim 1981 (lepidolite-1*M* from Radkovice)] and *C*2/*c* for $2M_1$ (Swanson and Bailey 1981) or $2M_2$ polytypes [Guggenheim 1981 (lepidolite-$2M_2$ from Radkovice)], suggest the presence of M1 layers. Hetero-trioctahedral Li-rich micas-1*M* (zinnwaldite-1*M*) refined by Guggenheim and Bailey (1977) and by Backhaus (1983) (lepidolite-1*M*) in *C*2 subgroup were built up of M2 layers and M1 layers, respectively. Furthermore, the refinement of a $2M_1$ polytype (zinnwaldite-$2M_1$), in the space group *Cc* (Rieder et al. 1996) indicates an octahedral cation

*E-mail: brigatti@unimo.it
†Deceased on January 8, 1998.

ordering similar to that reported by Guggenheim and Bailey (1977) for 1*M* polytype.

However, data are lacking on changes in geometrical and ordering parameters induced by variation in composition and degree of order for crystals in the K-Li-Fe-Al-Si trioctahedral mica system.

Here, we attempt to (1) characterize the crystal structure of 17 mica-1*M* crystals in the K-Li-Fe-Al-Si trioctahedral mica composition plane; (2) clarify the mechanisms of Li incorporation in the layer; (3) identify the ordering pattern of the octahedral sites.

## EXPERIMENTAL METHODS

### Samples

The mica crystals (Table 1) represent the binary joins siderophyllite-polylithionite and annite-siderophyllite. All crystals are from the shallow-seated to subvolcanic pegmatites of Precambrian Pikes Peak batholith, located in the southern Front Range of Colorado, west of Colorado Springs and south and southwest of Denver (Foord et al. 1995; Unruh et al. 1995; Kile and Foord 1998). The pegmatites in the southern part of the batholith host miarolitic cavities where micas were often associated with amazonite, smoky quartz, goethite, topaz, and fluorite (Foord et al. 1995).

### Chemical and optical determination

Significant compositional and distinct, sharp color zoning, resulting from primary growth fluctuations, are present in some mica crystals formed in miarolitic cavities (samples 140, 177, 54, 55, 114). Therefore, the crystals were initially examined by scanning electron microscope (Philips SEM XL-40 with an EDAX energy dispersive detector) by backscattered-electron imaging and X-ray maps to distinguish homogeneous portions.

Electron microprobe analyses were performed using a wavelength-dispersive ARL-SEMQ microprobe (operating conditions: 15 kV accelerating voltage, 15 nA sample current, and defocused electron beam of about 3 μm spot size). The F content was determined by the method reported by Foley (1989). Analyses and data reduction were done using the PROBE software package (Donovan 1995). Li content was determined by Emission Spectrometry Plasma (ICP, Varian Liberty 200). Then 25 mg of each sample were digested with a mixture of HF (38%) and $HNO_3$ (62%) in closed Teflon crucibles in a microwave. $(OH)^-$ was measured by thermogravimetric analysis in Ar gas flow to minimize the reaction $2FeO + 2(OH)^- \rightarrow Fe_2O_3 + H_2 + O^{2-}$, using a Seiko SSC 5200 thermal analyzer (heating rate 10 °C/min and flow rate 200 mL/min). The determination based on the weight loss observed in the temperature range 500–1100 °C was adjusted for the F content. The $Fe^{2+}$ amount (estimated measure standard deviation $\sigma < 4\%$) was estimated by a semi-micro-volumetric method (Meyrowitz 1970). The chemical formulae were based on $O_{24-x-y}(OH)_xF_y$. Chemical composition (Table 2) was determined by combining the microprobe results with structure refinement (for Li, OH, and $Fe^{2+}$).

Optical data (Table 3) were determined using a conventional petrographic microscope and calibrated immersion oils. Two of the refractive indices, $n_\beta$ and $n_\gamma$, were determined by grain mount on an approximately centered Bxa figure; $n_\alpha$ was determined using spindle stage methods to attain proper orientation of the X vibration direction. Determination of the refractive indices for lighter-colored micas was relatively straightforward, and the error is given as ±0.002, whereas determination of the indices of the darker and more pleochroic samples, i.e., those having indices above approximately 1.650, have errors of ±0.004. The optic axial angle was determined by Mallard's method, using an ocular micrometer. The $2V_X$ was calculated ($D = Kn_\beta \sin V$). For further details see Kile and Foord (1998).

### X-ray single-crystal diffraction

Crystals were examined by the precession method, and those belonging to 1*M* polytype were selected for cell dimensions and intensity data. In general, crystal quality was good, but in some cases [310] twinning, 1*Md* sequences and different polytypes (mostly 3*T*) were found.

X-ray diffraction data were collected on a Siemens automated four-circle diffractometer with rotating anode (graphite-monochromated Mo$K\alpha$ radiation of $\lambda = 0.71073$ Å at 52 kV and 140 mA operating conditions) using X-SCAN software (Siemens 1996). Reflection intensities ($+h$, $\pm k$, $\pm l$) were collected using the ω scan mode (scan window 2.2–3.8°) and corrected for Lorentz-polarization effects and for absorption using a complete ψ scan (0–360° at 10° intervals in φ) with more than five uniformly distributed reflections with regard to 2θ ($\chi > 80°$). The unit-cell parameters were determined from the setting angles of more than 50 reflections in the range $15 \le 2\theta \le 30°$. Details are given in Table 4. The crystal structure refinement [programs SHELX93 by Sheldrick (1993) and ORFLS

**TABLE 1.** Localities and associated minerals of the micas from Pikes Peak batholith, central Colorado

| Sample | Occurrence | Associated minerals |
|---|---|---|
| 114 | miarolitic cavity, Sentinel Rock | amazonite |
| 55 | miarolitic cavity, Wigwam Creek | amazonite, albite, smoky quartz, fluorite |
| 130 | miarolitic cavity, Devils Head area | amazonite, albite, smoky quartz, fluorite |
| 137 | miarolitic cavity, Lake George Ring complex | smoky quartz, microcline, albite |
| 104 | miarolitic cavity, Crystal Park area | amazonite, smoky quartz |
| 54 | miarolitic cavity, Harris Park | amazonite |
| 177 | miarolitic cavity, Wigwam Creek | amazonite, smoky quartz, albite |
| 140 | miarolitic cavity, Lake George Ring complex | amazonite, smoky quartz |
| 24 | miarolitic cavity, Wigwam Creek | amazonite, quartz, albite |
| 47 | quartz core, Lake George Ring complex | microcline |
| 103 | quartz core, Crystal Park | amazonite |
| 26 | quartz core, Wigwam Creek | quartz, K-feldspar, albite |
| 33 | massive quartz, Pikes Peak Granite | smoky quartz, albite |
| 120 | quartz core, Wigwam Creek | biotite |

by Busing et al. (1962)] started from atomic coordinates of the ideal space group *C*2/*m*. To check for possible ordering of the trivalent cations, the refinements were also carried out in the C2 subgroup, which leads to three independent M sites (M1, M2, and M3). For samples 114, 55a, 55b, 130, 137, 104, 54b, 177, 140, 24, 47, and 103 the refinements in *C*2 symmetry indicate that: (1) there are different features for M sites, primarily linked to differences in size and to a lesser extent in scattering power; (2) there is an improvement of the final R factors respect to that found for *C*2/*m* refinement; and, (3) there is no significant correlation noted by varying all the parameters together. On the contrary, samples 26, 33, and 120 showed no significant deviations from *C*2/*m* symmetry.

The atomic displacement factors were initially assigned to be isotropic. As the refinements progressed, scale factors, atomic positions, and cation occupancies were allowed to vary, and the atomic displacement factors were refined anisotropically. Scattering factors for neutral and ionized atoms were taken from the *International Tables of Crystallography* (Maslen et al. 1995; Creagh and McAuley 1995). Complete ionization of the cations at the M1, M2, M3 and A sites was adopted, whereas both neutral and ionized scattering factors were used for tetrahedral and anion sites (Brigatti and Davoli 1990). The initial scattering factors were $Fe^{2+}$ vs. $Al^{3+}$ for octahedral M sites, $K^{+}$ for interlayer A site, O vs. $O^{-2}$ for anion site, and a composite 75% Si to 25% Al vs. 75% $Si^{4+}$ to 25% $Al^{3+}$ for tetrahedral T sites. In the final part of the anisotropic refinement, scattering curves appropriate to the composition of each crystal (determined by microprobe analysis) were applied. The difference electron density maps (DED) at this stage did not reveal any obviously wrong atomic position or extra maxima that might indicate twinning or intergrowth structures. The number of unique reflections, the conventional discrepancy index as well as unit-cell parameters are reported in Table 4. Bond distances are in Table 5; selected tetrahedral, octahedral, and interlayer parameters are in Table 6. The mean electron counts of M sites and the M cation distribution are in Table 7. The final positional and displacement parameters (Table 8[1]), the observed and calculated structure factors (Table 9[1]) are deposited.

### Site population

The site population at M1, M2, and M3 sites was determined using both the results of structure refinements (i.e., the mean atomic number and the mean bond distances for M1, M2, and M3 sites) and chemical analysis (i.e., the atomic fractions of octahedral $Al^{3+}$,$Ti^{4+}$, $Fe^{3+}$, $Fe^{2+}$, $Mg^{2+}$, $Mn^{2+}$, $Zn^{2+}$, and $Li^{+}$) and taking into account the charge-balance requirements. For each species i, the best fraction $x_i$ was determined using a minimization procedure (based on the function FMINS pre-defined in MATLAB program library, Moler 1992) that identify the vector which best fits an over determined equation system **Ax** = **b** (where **A** is the matrix of coefficients (n × m), **b** is the vector of known terms and **x** is the vector of unknowns. Namely, let $\mathbf{A} = \{a_{ji}\}$, $\mathbf{x} = \{x_I\}$, and $\mathbf{b} = \{b_j\}$, the coefficient $a_{ji}$ represents the influence of species i over the balance expressed by equation number j (for example the atomic number or the ideal ⟨M-O⟩ distance of each species). In order to find the vector which best fits the system, the technique of least-squares was employed, calculating the minimum for the function $F(\mathbf{x}) = \mathbf{R}^{\mathbf{T}}*\mathbf{R}$, where $\mathbf{R} = \mathbf{A}*\mathbf{x}-\mathbf{b}$ and $\mathbf{R}^{\mathbf{T}}$ is the **R** transpose matrix. The accuracy of the fit between observed and calculated values was evaluated by the parameter

$$S = \sum_{j=1}^{n}\left(bj - \sum_{i=1}^{m}\left(a_{ji}x_i\right)\right)^2. \quad (1)$$

The ideal ⟨M-O⟩ octahedral distances calculated for each species by Weiss et al. (1985) were used, whereas for $Al^{3+}$ and vacancies the values obtained by Guggenheim (1981) (⟨M2-O⟩ of Tanakamiyama lepidolite-1*M*) and by Brigatti et al. (1998) (⟨M1-O⟩ of muscovite), respectively, were used. Vacancies were assigned to M1 and M3 sites, $Zn^{2+}$ was ignored or added to $Fe^{2+}$ because it never exceeded 0.02 apfu, and, excluding crystals 47, 33, and 120, $Ti^{4+}$ was added to $Fe^{3+}$. The site populations which best fit the observed chemical and structural data, giving S values in the range $9.0\cdot10^{-5}$ to $1.2\cdot10^{-3}$ are reported in Table 7.

## Results and discussion

### Chemistry

The variation in chemical composition compared to literature data is illustrated in Figure 1. As predicted by Foord et al.

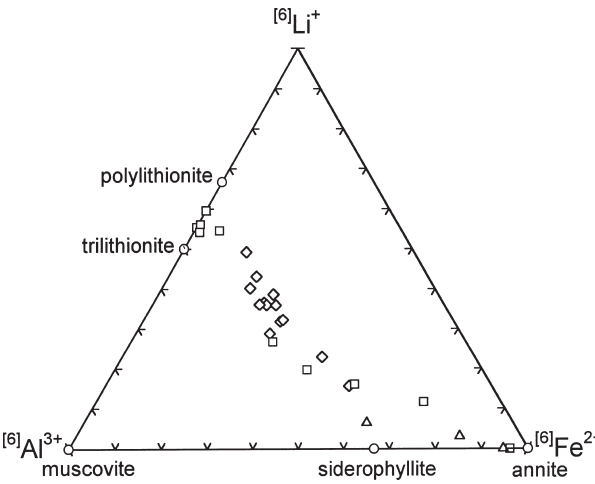


**Figure 1.** Ternary $^{[6]}Al^{3+} - {}^{[6]}Li^{+} - {}^{[6]}Fe^{2+}$ diagram (after Rieder et al. 1996) showing compositional data for micas from PPB batholith. Diamonds = Li-rich crystals [layer symmetry *C*12(1)]; triangles = Li-poor crystals [layer symmetry *C*12/*m*(1)]; squares = samples from literature (Hazen and Burnham 1973; Brown 1978; Guggenheim and Bailey 1977; Guggenheim 1981; Swanson and Bailey 1981; Backhaus 1983; Weiss et al. 1993; Rieder et al. 1996); circles = hypothetical end-members.

[1]For a copy of Tables 8 and 9, Document item AM-00-047, contact the Business Office of the Mineralogical Society of America for price information. Deposit items may also be available on the *American Mineralogist* web site at http://www.minsocam.org

**TABLE 2.** Chemical data for mica-1*M* crystals used in the structure refinement

| | Li-rich crystals Layer symmetry *C*12(1) | | | | | | | |
|---|---|---|---|---|---|---|---|---|
| | 114 | 55a | 55b | 130(1) | 130(2) | 137 | 104 | 54b |
| | **Weight percentages** | | | | | | | |
| $SiO_2$ | 49.54 | 47.47 | 47.18 | 44.73 | 45.28 | 43.64 | 45.15 | 45.27 |
| $TiO_2$ | 0.02 | 0.15 | 0.10 | 0.03 | 0.09 | 0.08 | 0.19 | 0.10 |
| $Al_2O_3$ | 18.05 | 20.07 | 19.36 | 19.70 | 19.52 | 21.22 | 20.06 | 20.21 |
| $Fe_2O_3$ | 0.87 | 0.96 | 1.08 | 1.65 | 1.06 | 1.30 | 2.56 | 2.14 |
| FeO | 6.75 | 8.86 | 9.02 | 11.43 | 11.57 | 10.96 | 10.44 | 9.97 |
| MgO | 0.02 | 0.09 | 0.05 | 0.20 | 0.20 | 0.11 | 0.12 | 0.08 |
| MnO | 0.63 | 0.64 | 0.75 | 0.99 | 1.00 | 1.19 | 0.18 | 1.02 |
| ZnO | 0.04 | 0.05 | 0.14 | 0.08 | 0.08 | 0.11 | 0.09 | 0.04 |
| CaO | b.d.t. | b.d.t. | b.d.t. | 0.07 | 0.07 | b.d.t. | 0.01 | b.d.t. |
| $Li_2O$ | 4.91 | 3.84 | 4.20 | 3.65 | 3.70 | 3.29 | 3.29 | 3.20 |
| $Na_2O$ | 0.04 | 0.01 | 0.08 | 0.11 | 0.11 | 0.16 | 0.14 | 0.14 |
| $Cs_2O$ | b.d.t. | 0.01 | 0.01 | b.d.t. | b.d.t. | 0.01 | b.d.t. | b.d.t. |
| $Rb_2O$ | 1.12 | 0.05 | 0.49 | b.d.t. | b.d.t. | b.d.t. | b.d.t. | 0.08 |
| $K_2O$ | 9.95 | 10.24 | 10.36 | 10.29 | 10.28 | 10.06 | 10.29 | 10.07 |
| $H_2O$ | 0.30 | 0.43 | 0.50 | 0.38 | 0.38 | 0.40 | 0.50 | 0.50 |
| F | 7.73 | 7.15 | 6.70 | 6.66 | 6.64 | 7.47 | 6.94 | 7.15 |
| Sum | 99.97 | 100.02 | 100.02 | 99.97 | 99.98 | 100.00 | 99.96 | 99.97 |
| | **Unit=cell content on the basis of $O_{24-x-y}(OH)_xF_y$** | | | | | | | |
| Si | 7.072 | 6.826 | 6.825 | 6.591 | 6.656 | 6.419 | 6.605 | 6.616 |
| $^{[4]}Al$ | 0.928 | 1.174 | 1.175 | 1.409 | 1.344 | 1.581 | 1.395 | 1.384 |
| $^{[6]}Al$ | 2.110 | 2.229 | 2.128 | 2.014 | 2.040 | 2.099 | 2.064 | 2.099 |
| Ti | 0.002 | 0.016 | 0.011 | 0.003 | 0.010 | 0.009 | 0.021 | 0.011 |
| $Fe^{3+}$ | 0.094 | 0.104 | 0.118 | 0.183 | 0.117 | 0.144 | 0.282 | 0.235 |
| $Fe^{2+}$ | 0.806 | 1.066 | 1.092 | 1.409 | 1.423 | 1.349 | 1.278 | 1.219 |
| Mg | 0.004 | 0.019 | 0.011 | 0.044 | 0.044 | 0.024 | 0.026 | 0.017 |
| Mn | 0.076 | 0.078 | 0.092 | 0.124 | 0.125 | 0.148 | 0.022 | 0.126 |
| Zn | 0.004 | 0.005 | 0.015 | 0.009 | 0.009 | 0.012 | 0.010 | 0.004 |
| Li | 2.821 | 2.222 | 2.445 | 2.164 | 2.189 | 1.947 | 1.937 | 1.882 |
| Ca | – | – | – | 0.011 | 0.011 | – | 0.002 | – |
| Na | 0.011 | 0.003 | 0.022 | 0.031 | 0.031 | 0.046 | 0.040 | 0.040 |
| Rb | 0.103 | 0.005 | 0.046 | – | – | – | – | 0.008 |
| K | 1.813 | 1.879 | 1.913 | 1.935 | 1.929 | 1.889 | 1.921 | 1.879 |
| OH | 0.285 | 0.412 | 0.482 | 0.373 | 0.372 | 0.487 | 0.487 | 0.487 |
| F | 3.492 | 3.253 | 3.067 | 3.106 | 3.089 | 3.477 | 3.212 | 3.307 |
| O | 20.223 | 20.335 | 20.451 | 20.521 | 20.539 | 20.036 | 20.301 | 20.206 |

*Note*: Labels (1) and (2) refer to different crystals from the same rock sample; labels a and b refer to different zones of the same crystal (a = core; b = rim); b.d.t.: below detection threshold.

(1995) and Kile and Foord (1998), the chemistry of the crystals examined varies widely within the field defined by annite, siderophyllite, and polylithionite. According to Rieder et al. (1998), these micas can be roughly classified as ferroan polylithionite, lithian siderophyllite, siderophyllite, and annite (Table 2). Some crystals present relatively high Rb content, variable K and low Zn, whereas the Ti content, which is very low and almost constant in ferroan polylithionite crystals, increases in lithian siderophyllite, siderophyllite, and annite to 0.495 apfu. The Si content (Fig. 2a) depends approximately linearly trend on $X_{Sid\text{-}Pl} = {}^{[6]}(Li+Al)/{}^{[6]}(Li+Al+Fe^{2+})$, which is consistent with the substitution $^{[6]}Fe^{2+}_{-1}{}^{[4]}Al_{-1}{}^{[4]}Si^{4+}{}^{[6]}Li$. As a result of Fe-F avoidance (Munoz 1984), F content increases toward polylithionite (Fig 2b). Therefore, siderophyllite being end-member, trioctahedral micas from PPB display both homovalent substitutions [e.g., $Mg^{2+}$, $Zn^{2+}$, and $Mn^{2+}$ for $Fe^{2+}$ in octahedral sites, $Rb^+$ and $Cs^+$ for $K^+$ in interlayer sites, and $F^-$ for $(OH)^-$ in anion sites] and heterovalent substitutions (e.g., $Li^+$ for $Fe^{2+}$ in octahedral sites and $Si^{4+}$ for $Al^{3+}$ in tetrahedral sites). Bearing charge balance and site occupancy in mind, the constraints governing the exchange mechanism can be nearly completely described by the vector $^{[6]}Fe^{2+}_{-1}{}^{[4]}Al^{3+}_{-1}{}^{[4]}Si^{4+}{}^{[6]}Li^+$, which links siderophyllite and polylithionite. The variation in composition of the samples investigated will, therefore, be described in terms of $X_{Sid\text{-}Pl}$ although other exchange vectors should be taken into account if the composition of these micas is to be completely described ( i.e., $^{[6]}R^{2+}_{-3}{}^{[6]}R^{3+}_{2}{}^{[6]}\square$, $^{[6]}R^{2+}_{-1}{}^{[4]}Si^{4+}_{-2}{}^{[6]}Ti^{4+}{}^{[4]}Al^{3+}_{2}$, $^{[6]}R^{2+}_{-2}{}^{[6]}Ti^{4+}{}^{[6]}\square$, $OH^-_{-1}F^-$, $^{[6]}R^{2+}_{-1}OH^-_{-2}{}^{[6]}Ti^{4+}O^{2-}_{2}$, and $^{[12]}K^+_{-1}{}^{[12]}Rb^+$, where $R^{3+}$ and $R^{2+}$ are trivalent and divalent cations, respectively).

## Crystal chemistry

Changes in the geometrical parameters induced by variation in composition and degree of order in the polylithionite-siderophyllite-annite field afford a complete description of the behavior of these micas. The lengths of unit-cell edges (Fig. 3) all decrease from annite to polylithionite, through siderophyllite. The lateral parameters *a*, and consequently *b* (Fig. 3a) correlate linearly with

$$X^*_{Sid-Pl} = \frac{\left(\langle Li-O\rangle^3 + \langle Al-O\rangle^3\right)\times X_{Li}}{\left(\langle Li-O\rangle^3 + \langle Al-O\rangle^3\right)\times X_{Li} + \left\langle Fe^{2+}-O\right\rangle^3 \times (1-X_{Li})} \quad (2)$$

where ⟨Li-O⟩, ⟨Al-O⟩, and ⟨$Fe^{2+}$-O⟩ are the ideal cation-anion bond distances and $X_{Li}$ is the ratio $^{[6]}Li/{}^{[6]}(Li+Fe^{2+})$. In contrast, c decreases mostly with $^{[6]}Al$ content (Fig. 3b) and shows a

**TABLE 2**—*Extended*

| | | | | | | | | |
|---|---|---|---|---|---|---|---|---|
| | | | | | | Li-poor crystals Layer symmetry *C*12/*m*(1) | | |
| 177 | 140(1) | 140(2) | 24 | 47 | 103 | 26 | 33 | 120 |
| **Weight percentages** | | | | | | | | |
| 43.41 | 42.73 | 43.57 | 44.41 | 38.81 | 41.80 | 36.40 | 36.66 | 37.40 |
| 0.09 | 0.44 | 0.45 | 0.10 | 1.72 | 0.55 | 0.39 | 1.70 | 3.92 |
| 18.85 | 21.05 | 19.94 | 20.44 | 18.88 | 18.46 | 19.86 | 12.61 | 10.02 |
| 4.31 | 0.69 | 0.94 | 0.81 | 1.58 | 1.61 | 3.98 | 2.50 | 3.39 |
| 10.40 | 13.00 | 12.95 | 12.48 | 21.17 | 18.46 | 24.06 | 31.46 | 32.60 |
| 0.08 | 0.47 | 0.48 | 0.03 | 0.30 | 0.20 | 0.80 | 0.01 | 0.83 |
| 1.02 | 0.94 | 0.95 | 1.26 | 1.18 | 0.80 | 0.05 | 1.10 | 0.14 |
| 0.22 | 0.19 | 0.20 | 0.03 | 0.29 | 0.22 | 0.12 | b.d.t. | b.d.t. |
| b.d.t. | b.d.t. | b.d.t. | b.d.t. | b.d.t. | b.d.t. | b.d.t. | b.d.t. | b.d.t. |
| 2.88 | 2.86 | 2.85 | 2.55 | 1.29 | 2.01 | 0.52 | 0.24 | b.d.t. |
| 0.28 | 0.10 | 0.10 | 0.24 | 0.09 | 0.24 | 0.30 | 0.09 | 0.06 |
| b.d.t. | b.d.t. | b.d.t. | b.d.t. | b.d.t. | b.d.t. | b.d.t. | b.d.t. | b.d.t. |
| 0.05 | b.d.t. | b.d.t. | 1.92 | b.d.t. | 0.03 | 0.44 | b.d.t. | b.d.t. |
| 9.92 | 10.10 | 10.07 | 8.62 | 9.80 | 10.00 | 9.23 | 9.27 | 9.20 |
| 0.30 | 0.50 | 0.50 | 0.35 | 0.54 | 0.30 | 0.31 | 0.30 | 1.41 |
| 8.16 | 6.90 | 6.98 | 6.74 | 4.33 | 5.30 | 3.53 | 4.07 | 0.99 |
| 99.97 | 99.97 | 99.98 | 99.98 | 99.98 | 99.98 | 99.99 | 100.01 | 99.96 |
| **Unit cell content on the basis of $O_{24-x-y}(OH)_xF_y$** | | | | | | | | |
| 6.458 | 6.349 | 6.470 | 6.623 | 6.114 | 6.450 | 5.885 | 6.187 | 6.273 |
| 1.542 | 1.651 | 1.530 | 1.377 | 1.886 | 1.550 | 2.115 | 1.813 | 1.727 |
| 1.764 | 2.037 | 1.961 | 2.217 | 1.621 | 1.809 | 1.670 | 0.697 | 0.255 |
| 0.010 | 0.049 | 0.050 | 0.011 | 0.204 | 0.064 | 0.047 | 0.216 | 0.495 |
| 0.483 | 0.077 | 0.105 | 0.091 | 0.187 | 0.187 | 0.484 | 0.318 | 0.428 |
| 1.295 | 1.616 | 1.609 | 1.557 | 2.791 | 2.384 | 3.254 | 4.443 | 4.576 |
| 0.018 | 0.104 | 0.106 | 0.007 | 0.071 | 0.046 | 0.193 | 0.003 | 0.208 |
| 0.129 | 0.118 | 0.120 | 0.159 | 0.158 | 0.105 | 0.007 | 0.157 | 0.020 |
| 0.024 | 0.021 | 0.022 | 0.003 | 0.034 | 0.025 | 0.014 | – | – |
| 1.724 | 1.710 | 1.703 | 1.530 | 0.818 | 1.248 | 0.338 | 0.163 | – |
| – | – | – | – | – | – | – | – | – |
| 0.081 | 0.029 | 0.029 | 0.069 | 0.028 | 0.072 | 0.094 | 0.029 | 0.020 |
| 0.005 | – | – | 0.184 | – | 0.003 | 0.046 | – | – |
| 1.884 | 1.916 | 1.909 | 1.641 | 1.971 | 1.970 | 1.905 | 1.997 | 1.970 |
| 0.297 | 0.495 | 0.495 | 0.348 | 0.567 | 0.308 | 0.334 | 0.337 | 1.575 |
| 3.841 | 3.244 | 3.280 | 3.181 | 2.159 | 2.588 | 1.806 | 2.174 | 0.525 |
| 19.862 | 20.261 | 20.225 | 20.471 | 21.274 | 21.104 | 21.860 | 21.489 | 21.900 |

**TABLE 3.** Optical data for mica-1*M* samples from Pikes Peak batholith, central Colorado

| Sample | $n_\alpha$ | $n_\beta$ | $n_\gamma$ | $2V_X$ |
|---|---|---|---|---|
| **Li-rich crystals [layer symmetry *C*12(1)]** | | | | |
| 114 | 1.541 | 1.563 | 1.564 | 32.9 |
| 55a | 1.548 | 1.572 | 1.574 | 29.2 |
| 55b | 1.547 | 1.569 | 1.570 | 26.5 |
| 130 | 1.551 | 1.577 | 1.578 | 29.7 |
| 137 | 1.551 | 1.581 | 1.583 | 29.8 |
| 104 | 1.553 | 1.581 | 1.583 | 29.1 |
| 54b | 1.557 | 1.577 | 1.579 | 29.2 |
| 177 | 1.552 | 1.583 | 1.584 | 25.2 |
| 140 | 1.556 | 1.590 | 1.591 | 26.1 |
| 24 | 1.549 | 1.581 | 1.583 | 29.7 |
| 47 | 1.583 | 1.636 | 1.637 | 13.1 |
| 103 | 1.563 | 1.603 | 1.603 | 6.4 |
| **Li-poor crystals [layer symmetry *C*12/*m*(1)]** | | | | |
| 26 | 1.591 | 1.651 | 1.652 | 7.4 |
| 33 | 1.594 | 1.667 | 1.667 | 9.4 |
| 120 | 1.615 | 1.702 | 1.702 | 12.7 |

*Note*: Labels a and b as in Table 2.

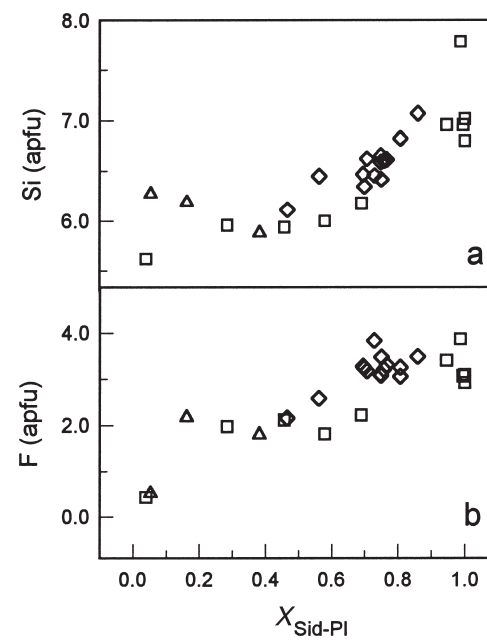


**FIGURE 2.** Variation of (**a**) Si and (**b**) F content with $X_{Sid\text{-}Pl}$ [$X_{sid\text{-}Pl} = {}^{[6]}(Li+Al) / {}^{[6]}(Li+Al+Fe^{2+})$] in micas from PPB batholith. Symbols and samples as in Figure 1.

**TABLE 4.** Details on the data collection and structure refinement of the mica-1*M* crystals

| Samples | Crystal dimension ($mm^3$) | Range 2θ (°) | *N* | $R_{obs}$ ×100 | Unit-cell parameters *a* (Å) | *b* (Å) | *c* (Å) | β (°) | *V* ($Å^3$) |
|---|---|---|---|---|---|---|---|---|---|
| **Li-rich crystals [layer symmetry *C*12(1)]** | | | | | | | | | |
| 114 | 0.12 × 0.16 × 0.02 | 3.5–75 | 2768 | 3.35 | 5.262(1) | 9.085(2) | 10.099(2) | 100.72(1) | 474.4 |
| 55a | 0.04 × 0.01 × 0.04 | 3.5–60 | 1394 | 3.74 | 5.270(1) | 9.092(1) | 10.080(2) | 100.70(1) | 474.6 |
| 55b | 0.20 × 0.30 × 0.02 | 3.5–65 | 1223 | 3.21 | 5.263(1) | 9.085(1) | 10.078(1) | 100.75(1) | 473.4 |
| 130(1) | 0.12 × 0.22 × 0.016 | 3.5–60 | 1458 | 2.96 | 5.290(1) | 9.128(1) | 10.093(1) | 100.80(1) | 478.7 |
| 130(2) | 0.12 × 0.18 × 0.02 | 3.5–75 | 2420 | 3.86 | 5.275(2) | 9.105(2) | 10.084(1) | 100.70(1) | 475.9 |
| 137 | 0.016 × 0.24 × 0.004 | 3.5–65 | 1418 | 3.63 | 5.279(1) | 9.114(2) | 10.077(2) | 100.79(1) | 476.3 |
| 104 | 0.40 × 0.40 × 0.02 | 3.5–65 | 1574 | 3.34 | 5.285(1) | 9.122(2) | 10.101(2) | 100.85(1) | 478.3 |
| 54b | 0.06 × 0.06 × 0.01 | 4–65 | 1712 | 3.78 | 5.283(1) | 9.123(2) | 10.072(2) | 100.76(1) | 476.9 |
| 177 | 0.12 × 0.16 × 0.01 | 3.5–75 | 1997 | 3.39 | 5.288(1) | 9.133(1) | 10.088(1) | 100.81(1) | 478.6 |
| 140(1) | 0.20 × 0.20 × 0.02 | 3.5–65 | 1826 | 2.89 | 5.283(1) | 9.118(1) | 10.092(1) | 100.78(1) | 477.6 |
| 140(2) | 0.20 × 0.22 × 0.02 | 3.5–65 | 1876 | 2.73 | 5.297(1) | 9.146(1) | 10.102(1) | 100.81(1) | 480.7 |
| 24 | 0.50 × 0.80 × 0.005 | 3.5–65 | 1708 | 3.72 | 5.295(1) | 9.139(2) | 10.077(2) | 100.83(2) | 479.0 |
| 47 | 0.14 × 0.50 × 0.02 | 3.5–75 | 2819 | 3.31 | 5.339(1) | 9.233(1) | 10.135(2) | 100.73(1) | 490.9 |
| 103 | 0.34 × 0.36 × 0.01 | 3.5–65 | 1542 | 3.63 | 5.300(1) | 9.144(1) | 10.089(2) | 100.74(1) | 480.4 |
| **Li-poor crystals [layer symmetry *C*12/*m*(1)]** | | | | | | | | | |
| 26 | 0.16 × 0.30 × 0.01 | 3.5–70 | 615 | 3.26 | 5.358(2) | 9.280(3) | 10.151(2) | 100.10(2) | 496.9 |
| 33 | 0.30 × 0.30 × 0.02 | 3.5–65 | 819 | 3.59 | 5.372(1) | 9.313(1) | 10.204(1) | 100.52(1) | 501.9 |
| 120 | 0.14 × 0.28 × 0.01 | 3.5–60 | 624 | 2.55 | 5.384(1) | 9.324(1) | 10.254(1) | 100.86(1) | 505.5 |

*Note:* Labels (1), (2), a, and b as in Table 2. N is the number of unique reflections; $R_{obs}$ is the structure refinement agreement factor.

**TABLE 5A.** Bond distances (Å) for Li-rich crystals [layer symmetry *C*12(1)]

| Sample: | 114 | 55a | 55b | 130(1) | 130(2) | 137 | 104 | 54b | 177 |
|---|---|---|---|---|---|---|---|---|---|
| **Tetrahedron (T1)** | | | | | | | | | |
| T1-O1 | 1.631(3) | 1.640(5) | 1.640(5) | 1.646(3) | 1.641(3) | 1.642(5) | 1.643(3) | 1.640(4) | 1.646(4) |
| T1-O2 | 1.642(2) | 1.639(4) | 1.634(4) | 1.644(3) | 1.636(3) | 1.641(5) | 1.640(3) | 1.639(3) | 1.644(3) |
| T1-O22 | 1.635(2) | 1.649(4) | 1.640(4) | 1.646(3) | 1.650(3) | 1.635(4) | 1.644(2) | 1.648(3) | 1.646(3) |
| T1-O3 | 1.621(2) | 1.635(3) | 1.623(3) | 1.650(3) | 1.635(2) | 1.636(4) | 1.648(2) | 1.640(3) | 1.636(3) |
| <T1-O> | 1.632 | 1.641 | 1.634 | 1.647 | 1.641 | 1.639 | 1.644 | 1.642 | 1.643 |
| **Tetrahedron (T11)** | | | | | | | | | |
| T11-O1 | 1.644(3) | 1.633(5) | 1.635(5) | 1.635(3) | 1.632(3) | 1.635(5) | 1.640(3) | 1.641(4) | 1.632(4) |
| T11-O2 | 1.647(2) | 1.637(4) | 1.640(4) | 1.641(3) | 1.638(3) | 1.650(4) | 1.638(3) | 1.639(3) | 1.640(3) |
| T11-O22 | 1.639(2) | 1.643(4) | 1.648(4) | 1.648(3) | 1.649(3) | 1.643(5) | 1.647(3) | 1.642(3) | 1.644(3) |
| T11-O33 | 1.629(2) | 1.625(3) | 1.620(2) | 1.637(2) | 1.629(2) | 1.634(4) | 1.633(2) | 1.634(2) | 1.646(3) |
| <T11-O> | 1.640 | 1.635 | 1.636 | 1.640 | 1.637 | 1.641 | 1.640 | 1.639 | 1.641 |
| **Octahedron (M1)** | | | | | | | | | |
| M1-O3 (×2) | 2.117(2) | 2.118(4) | 2.113(4) | 2.129(3) | 2.130(3) | 2.141(4) | 2.136(2) | 2.141(4) | 2.139(3) |
| M1-O33 (×2) | 2.130(2) | 2.124(4) | 2.140(4) | 2.128(3) | 2.120(3) | 2.115(4) | 2.133(3) | 2.129(4) | 2.120(3) |
| M1-O4 (×2) | 2.124(1) | 2.132(2) | 2.133(2) | 2.128(2) | 2.124(2) | 2.132(2) | 2.131(2) | 2.138(2) | 2.132(2) |
| <M1-O> | 2.124 | 2.125 | 2.129 | 2.128 | 2.125 | 2.129 | 2.133 | 2.136 | 2.130 |
| **Octahedron (M2)** | | | | | | | | | |
| M2-O3 (×2) | 2.130(2) | 1.900(4) | 1.899(3) | 1.896(3) | 1.893(3) | 1.887(5) | 1.898(3) | 1.890(3) | 1.899(3) |
| M2-O33 (×2) | 2.110(2) | 1.908(3) | 1.896(3) | 1.908(2) | 1.912(2) | 1.903(3) | 1.907(2) | 1.899(2) | 1.903(2) |
| M2-O4 (×2) | 2.127(2) | 1.857(3) | 1.850(3) | 1.865(3) | 1.864(3) | 1.864(4) | 1.865(2) | 1.860(3) | 1.870(3) |
| <M2-O> | 2.122 | 1.888 | 1.882 | 1.890 | 1.890 | 1.885 | 1.890 | 1.883 | 1.891 |
| **Octahedron (M3)** | | | | | | | | | |
| M3-O3 (×2) | 1.904(1) | 2.111(3) | 2.114(3) | 2.117(2) | 2.114(2) | 2.120(3) | 2.102(2) | 2.121(2) | 2.122(2) |
| M3-O33 (×2) | 1.892(2) | 2.122(4) | 2.120(4) | 2.131(3) | 2.129(3) | 2.139(5) | 2.126(3) | 2.138(3) | 2.134(3) |
| M3-O4 (×2) | 1.860(2) | 2.139(4) | 2.146(4) | 2.132(3) | 2.131(3) | 2.133(4) | 2.141(2) | 2.138(3) | 2.136(3) |
| <M3-O> | 1.885 | 2.124 | 2.127 | 2.127 | 2.125 | 2.131 | 2.123 | 2.132 | 2.131 |
| **Interlayer cation** | | | | | | | | | |
| A-O1 (×2) | 3.042(1) | 3.040(2) | 3.035(3) | 3.021(2) | 3.038(2) | 3.032(2) | 3.029(2) | 3.048(2) | 3.033(2) |
| A-O1' (×2) | 3.226(2) | 3.230(3) | 3.226(3) | 3.275(2) | 3.242(2) | 3.243(3) | 3.261(2) | 3.228(2) | 3.257(2) |
| A-O2 (×2) | 2.997(3) | 3.035(4) | 3.025(4) | 3.021(3) | 3.038(3) | 3.034(5) | 3.031(3) | 3.043(3) | 3.035(4) |
| A-O2' (×2) | 3.134(2) | 3.233(4) | 3.239(4) | 3.268(3) | 3.242(3) | 3.225(5) | 3.260(3) | 3.232(3) | 3.253(3) |
| A-O22 (×2) | 3.047(2) | 2.992(4) | 3.005(4) | 2.985(3) | 2.992(3) | 2.988(5) | 2.995(3) | 3.009(3) | 2.996(4) |
| A-O22' (×2) | 3.225(2) | 3.135(3) | 3.115(4) | 3.166(3) | 3.135(3) | 3.160(5) | 3.158(3) | 3.125(3) | 3.156(3) |
| $<A-O>_{inner}$ | 3.029 | 3.022 | 3.022 | 3.009 | 3.023 | 3.018 | 3.018 | 3.033 | 3.021 |
| $<A-O>_{outer}$ | 3.195 | 3.199 | 3.193 | 3.236 | 3.206 | 3.209 | 3.226 | 3.195 | 3.222 |

*Note:* Labels (1), (2), a, and b as in Table 2.

negative correlation with $X^{*}_{Sid\text{-}Pl}$ only in the range $0 < X^{*}_{Sid\text{-}Pl} < 0.5$. For the angle β, only the difference between the values of *C*12(1) (lithian siderophyllite and ferroan polylithionite crystals) and *C*12/*m*(1) (siderophyllite crystals) is larger than the estimated standard deviations ($\Delta\beta \geq 5\sigma$).

Kile and Foord (1998) demonstrated that $n_\beta$ provides an excellent indicator of geochemical differentiation within PPB, and its determination can provide an unambiguous assessment of paragenesis. As observed by Rieder et al. (1971) and Gottesmann and Tischendorf (1978), Li-Fe mica cell dimensions correlate positively with the refractive indices $n_\beta$ and $n_\gamma$, which decrease as Fe decreases and Li increases: $n_\beta$ varies from 1.563 (sample 114) to 1.702 (sample 120) and is correlated with lateral unit-cell parameters (e.g., *a* vs. $n_\beta$, r = 0.982) as well as with $Fe_{total}$ (r = 0.986) and $X^{*}_{Sid\text{-}Pl}$ (r = –0.984).

The most important features in the samples studied are the differences in the dimensions and scattering power of octahedral M2 and M3 sites, which lead to a symmetry reduction from *C*12/*m*(1) to *C*12(1) diperiodic group in ferroan polylithionite and lithian siderophyllite. In a ferroan polylithionite (sample 144) the octahedral mean bond distances are ⟨M1-O⟩ ≅ ⟨M3-

**TABLE 5A**—*Extended*

| 140(1) | 140(2) | 24 | 47 | 103 |
|---|---|---|---|---|
| | | | | |
| 1.646(3) | 1.646(2) | 1.640(4) | 1.655(5) | 1.640(5) |
| 1.638(3) | 1.643(2) | 1.638(3) | 1.655(4) | 1.646(4) |
| 1.649(2) | 1.647(2) | 1.648(3) | 1.653(4) | 1.648(4) |
| 1.638(2) | 1.647(2) | 1.655(3) | 1.669(2) | 1.636(4) |
| 1.643 | 1.646 | 1.645 | 1.658 | 1.643 |
| | | | | |
| 1.633(3) | 1.637(2) | 1.640(4) | 1.641(5) | 1.637(3) |
| 1.640(3) | 1.645(2) | 1.640(3) | 1.645(4) | 1.637(4) |
| 1.647(3) | 1.651(2) | 1.646(3) | 1.637(4) | 1.655(4) |
| 1.629(2) | 1.639(1) | 1.646(2) | 1.626(3) | 1.636(3) |
| 1.637 | 1.643 | 1.643 | 1.637 | 1.641 |
| | | | | |
| 2.137(3) | 2.135(2) | 2.131(3) | 2.130(4) | 2.132(4) |
| 2.130(3) | 2.136(2) | 2.127(3) | 2.123(4) | 2.128(4) |
| 2.133(2) | 2.135(1) | 2.144(2) | 2.124(2) | 2.133(2) |
| 2.133 | 2.135 | 2.134 | 2.126 | 2.131 |
| | | | | |
| 1.897(3) | 1.905(2) | 1.888(3) | 2.005(4) | 1.933(4) |
| 1.909(2) | 1.912(1) | 1.901(2) | 2.044(4) | 1.934(3) |
| 1.867(2) | 1.871(2) | 1.867(3) | 2.003(5) | 1.882(4) |
| 1.891 | 1.896 | 1.885 | 2.017 | 1.916 |
| | | | | |
| 2.116(2) | 2.119(1) | 2.121(2) | 2.074(3) | 2.122(3) |
| 2.134(3) | 2.134(2) | 2.134(3) | 2.118(4) | 2.126(4) |
| 2.136(2) | 2.141(1) | 2.144(3) | 2.064(5) | 2.139(4) |
| 2.129 | 2.131 | 2.133 | 2.085 | 2.129 |
| | | | | |
| 3.042(2) | 3.038(1) | 3.026(2) | 3.066(1) | 3.055(2) |
| 3.243(2) | 3.262(1) | 3.265(2) | 3.256(2) | 3.234(3) |
| 3.044(3) | 3.040(2) | 3.033(3) | 3.069(4) | 3.051(4) |
| 3.239(3) | 3.252(2) | 3.263(3) | 3.237(4) | 3.236(4) |
| 2.997(3) | 3.001(2) | 2.986(3) | 3.075(4) | 3.022(4) |
| 3.141(3) | 3.157(2) | 3.161(3) | 3.180(4) | 3.132(4) |
| 3.028 | 3.026 | 3.015 | 3.070 | 3.043 |
| 3.208 | 3.224 | 3.230 | 3.224 | 3.201 |

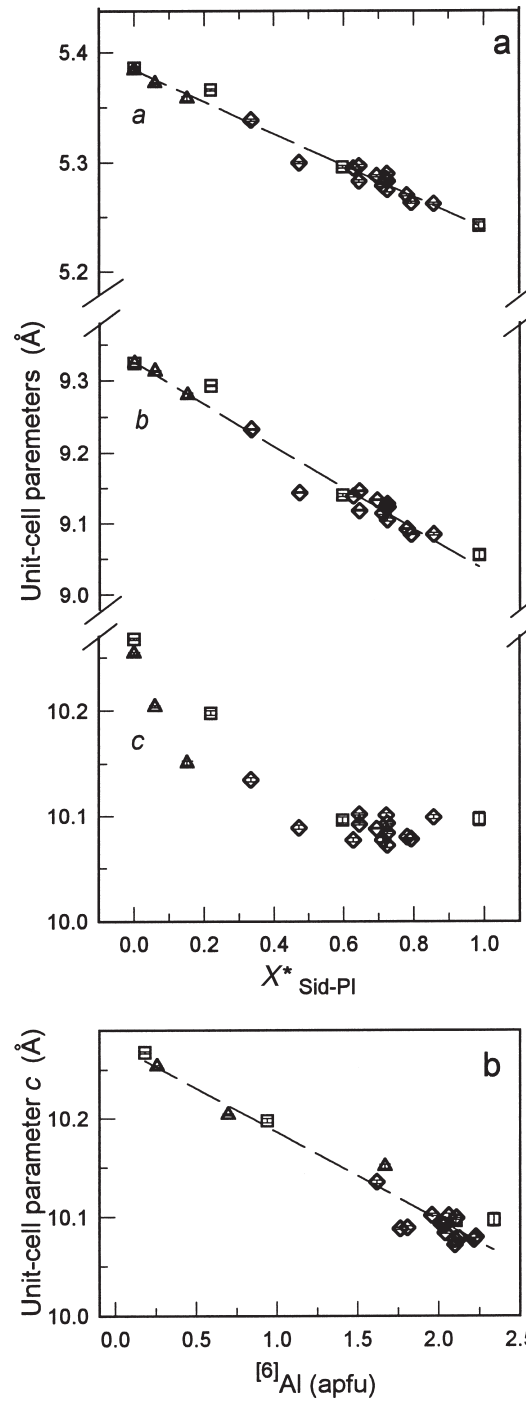


**FIGURE 3.** Compositional dependence of (**a**) unit-cell parameters a, b, c (Å) with $X^{*}_{Sid\text{-}Pl}$ (Eq. 2) and (**b**) of unit-cell parameter *c* (Å) with $^{[6]}$Al (apfu). Diamonds = Li-rich crystals [layer symmetry *C*12(1)]; triangles = Li-poor crystals [layer symmetry *C*12/*m*(1)]; squares = 1*M* polytype crystals from literature [Hazen and Burnham 1973 (annite); Guggenheim and Bailey 1977; Guggenheim 1981 ("lepidolite"-1*M* from Tanakamiyama); Weiss et al. 1993]. Error bars are reported for unit-cell parameters. Dashed lines represent regression equations [a(Å) = $-0.144 \cdot X^{*}_{Sid\text{-}Pl} + 5.384$ (correlation coefficient r = 0.989); b (Å) = $-0.290 \cdot X^{*}_{Sid\text{-}Pl} + 9.325$ (r = 0.985); c (Å) = $-8.95 \cdot 10^{-2} \cdot {}^{[6]}Al + 10.276$ (r = 0.970)].

**TABLE 5B.** Bond distances (Å) for Li-poor crystals [layer symmetry *C*12/*m*(1)]

| Sample: | 26 | 33 | 120 |
|---|---|---|---|
| | **Tetrahedron** | | |
| T1-O1 | 1.659(2) | 1.653(1) | 1.658(1) |
| T1-O2 | 1.652(3) | 1.663(2) | 1.656(2) |
| T1-O2' | 1.650(3) | 1.646(2) | 1.655(2) |
| T1-O3 | 1.710(2) | 1.662(2) | 1.664(2) |
| <T1-O> | 1.668 | 1.656 | 1.658 |
| | **Octahedron (M1)** | | |
| M1-O3 (×4) | 2.037(3) | 2.103(2) | 2.122(2) |
| M1-O4 (×2) | 2.104(3) | 2.120(3) | 2.107(3) |
| <M1-O> | 2.059 | 2.109 | 2.117 |
| | **Octahedron (M2)** | | |
| M2-O3 (×2) | 2.081(3) | 2.097(2) | 2.110(2) |
| M2-O3' (×2) | 2.075(3) | 2.102(2) | 2.108(2) |
| M2-O4 (×2) | 2.105(2) | 2.100(2) | 2.075(2) |
| <M2-O> | 2.087 | 2.100 | 2.098 |
| | **Interlayer cation** | | |
| A-O1 (×2) | 3.047(4) | 3.102(3) | 3.090(3) |
| A-O1' (×2) | 3.276(4) | 3.227(3) | 3.265(3) |
| A-O2 (×4) | 3.053(3) | 3.132(2) | 3.169(2) |
| A-O2' (×4) | 3.280(3) | 3.203(2) | 3.186(2) |
| $\langle A\text{-}O\rangle_{inner}$ | 3.051 | 3.122 | 3.143 |
| $\langle A\text{-}O\rangle_{outer}$ | 3.279 | 3.211 | 3.212 |

O⟩ > ⟨M2-O⟩ whereas in lithian siderophyllite and other ferroan polylithionite crystals ⟨M1-O⟩ ≅ ⟨M2-O⟩ > ⟨M3-O⟩ (Table 5a). Differences in mean bond lengths between M2 and M3 sites ($\Delta\langle M\text{-}O\rangle_{M2,\,M3}$) are nearly constant ($\Delta\langle M\text{-}O\rangle_{M2,\,M3}$ = 0.24 Å) for crystals with $X_{Sid\text{-}Pl} \geq 0.69$, whereas they decrease in samples 103 ($\Delta\langle M\text{-}O\rangle_{M2,\,M3}$ = 0.21 Å, $X_{Sid\text{-}Pl}$ = 0.56) and 47 ($\Delta\langle M\text{-}O\rangle_{M2,\,M3}$ = 0.07 Å, $X_{Sid\text{-}Pl}$ = 0.47). The refined scattering powers (Table 7a) for M1, M2, and M3 sites suggest both hetero- and meso-octahedral character (Ďurovič et al. 1984; Ďurovič 1994), the calculated mean atomic numbers being M1 ≠ M2 ≠ M3 [crystals: 114, 55a, 55b, 130(1), 137, 104, 54b, 177, 140(2), 24, 47, 103], M1 = M3 < M2 [crystal 130(2)], or M2 = M3 < M1 [crystal 140(1)]. Besides, Li-rich crystals with *C*12(1) layer symmetry were built up of M2 layers with the exception of crystal 140(1).

The ordering scheme in octahedral M2 and M3 can be specified in terms of ⟨M-O⟩ bond lengths by the ordering parameters $Q_{M2,\,M3}$ (Carpenter et al. 1990):

**TABLE 6A.** Selected parameters derived from structure refinement for Li-rich crystals [layer symmetry *C*12(1)]

| | 114 | 55a | 55b | 130(1) | 130(2) | 137 | 104 | 54b | 177 | 140(1) | 140(2) | 24 | 47 | 103 |
|---|---|---|---|---|---|---|---|---|---|---|---|---|---|---|
| | | | | | | | **Tetrahedral parameters** | | | | | | | |
| α (°) | 3.71 | 3.95 | 3.82 | 5.04 | 4.09 | 4.25 | 4.62 | 3.58 | 4.46 | 4.00 | 4.36 | 4.75 | 3.40 | 3.49 |
| Δz (Å) | 0.131 | 0.134 | 0.135 | 0.129 | 0.144 | 0.109 | 0.130 | 0.133 | 0.128 | 0.137 | 0.127 | 0.141 | 0.058 | 0.125 |
| $\tau_{T1}$ (°) | 111.93 | 111.75 | 111.95 | 111.23 | 111.68 | 111.64 | 111.38 | 111.53 | 111.28 | 111.52 | 111.32 | 111.09 | 110.50 | 111.31 |
| $TAV_{T1}$ (°²) | 7.78 | 6.81 | 8.21 | 4.22 | 6.45 | 6.44 | 4.80 | 5.95 | 4.43 | 5.50 | 4.56 | 3.63 | 2.15 | 4.62 |
| $TQE_{T1}$ | 1.0018 | 1.0016 | 1.0019 | 1.0011 | 1.0015 | 1.0016 | 1.0012 | 1.0015 | 1.0010 | 1.0013 | 1.0011 | 1.0010 | 1.0006 | 1.0011 |
| VolumeT1 (Å³) | 2.226 | 2.260 | 2.234 | 2.287 | 2.260 | 2.252 | 2.276 | 2.265 | 2.272 | 2.271 | 2.285 | 2.284 | 2.335 | 2.269 |
| $\tau_{T11}$ (°) | 111.92 | 111.74 | 111.84 | 111.32 | 111.60 | 111.52 | 111.38 | 111.49 | 111.24 | 111.57 | 111.30 | 111.05 | 110.46 | 111.33 |
| $TAV_{T11}$ (°²) | 7.88 | 6.67 | 7.41 | 4.51 | 5.77 | 5.66 | 4.79 | 5.44 | 4.16 | 5.65 | 4.38 | 3.26 | 1.92 | 4.55 |
| $TQE_{T11}$ | 1.0018 | 1.0015 | 1.0017 | 1.0011 | 1.0014 | 1.0013 | 1.0011 | 1.0013 | 1.0011 | 1.0013 | 1.0011 | 1.0008 | 1.0005 | 1.0011 |
| VolumeT11 (Å³) | 2.256 | 2.234 | 2.240 | 2.261 | 2.246 | 2.262 | 2.257 | 2.255 | 2.263 | 2.247 | 2.272 | 2.274 | 2.250 | 2.261 |
| | | | | | | | **Octahedral parameters** | | | | | | | |
| $\psi_{M1}$ (°) | 60.59 | 60.59 | 60.57 | 60.83 | 60.66 | 60.70 | 60.80 | 60.75 | 60.73 | 60.63 | 60.73 | 60.90 | 59.81 | 60.37 |
| $\psi_{M2}$ (°) | 60.56 | 56.45 | 56.23 | 56.71 | 56.58 | 56.43 | 56.60 | 56.35 | 56.58 | 56.42 | 56.59 | 56.59 | 57.99 | 56.64 |
| $\psi_{M3}$ (°) | 56.41 | 60.57 | 60.54 | 60.81 | 60.66 | 60.72 | 60.65 | 60.70 | 60.74 | 60.57 | 60.67 | 60.88 | 59.16 | 60.34 |
| $OQE_{M1}$ | 1.0270 | 1.0269 | 1.0274 | 1.0289 | 1.0274 | 1.0283 | 1.0285 | 1.0287 | 1.0283 | 1.0274 | 1.0280 | 1.0297 | 1.0169 | 1.0244 |
| $OQE_{M2}$ | 1.0270 | 1.0022 | 1.0017 | 1.0028 | 1.0025 | 1.0024 | 1.0025 | 1.0020 | 1.0026 | 1.0021 | 1.0024 | 1.0025 | 1.0073 | 1.0026 |
| $OQE_{M3}$ | 1.0022 | 1.0271 | 1.0274 | 1.0288 | 1.0275 | 1.0284 | 1.0279 | 1.0285 | 1.0283 | 1.0271 | 1.0278 | 1.0298 | 1.0136 | 1.0244 |
| $OAV_{M1}$ (°²) | 90.25 | 89.96 | 91.67 | 95.86 | 91.40 | 94.34 | 94.65 | 95.84 | 94.10 | 91.27 | 92.98 | 98.71 | 55.03 | 81.29 |
| $OAV_{M2}$ (°²) | 90.03 | 6.98 | 5.53 | 9.31 | 8.25 | 7.93 | 8.35 | 6.51 | 8.68 | 7.04 | 8.10 | 8.51 | 24.09 | 8.34 |
| $OAV_{M3}$ (°²) | 7.13 | 90.20 | 91.63 | 95.55 | 91.55 | 94.57 | 92.87 | 95.37 | 94.21 | 90.45 | 92.35 | 98.90 | 45.24 | 81.33 |
| $Volume_{M1}$ (Å³) | 12.270 | 12.289 | 12.359 | 12.323 | 12.271 | 12.346 | 12.407 | 12.454 | 12.363 | 12.436 | 12.458 | 12.399 | 12.493 | 12.439 |
| $Volume_{M2}$(Å³) | 12.247 | 8.949 | 8.863 | 8.961 | 8.959 | 8.897 | 8.969 | 8.878 | 8.977 | 8.989 | 9.053 | 8.899 | 10.828 | 9.345 |
| $Volume_{M3}$(Å³) | 8.906 | 12.272 | 12.316 | 12.284 | 12.275 | 12.366 | 12.245 | 12.396 | 12.369 | 12.354 | 12.390 | 12.387 | 11.844 | 12.402 |
| $e_u/e_s$ (M1) | 1.148 | 1.148 | 1.148 | 1.155 | 1.149 | 1.151 | 1.153 | 1.152 | 1.152 | 1.149 | 1.151 | 1.156 | 1.129 | 1.142 |
| $e_u/e_s$ (M2) | 1.147 | 1.043 | 1.037 | 1.049 | 1.045 | 1.042 | 1.046 | 1.040 | 1.046 | 1.042 | 1.046 | 1.046 | 1.082 | 1.047 |
| $e_u/e_s$ (M3) | 1.027 | 1.147 | 1.146 | 1.154 | 1.150 | 1.151 | 1.149 | 1.151 | 1.152 | 1.147 | 1.150 | 1.155 | 1.111 | 1.140 |
| | | | | | | | **Sheet thickness (Å)** | | | | | | | |
| Tetrahedral | 2.251 | 2.249 | 2.246 | 2.254 | 2.252 | 2.250 | 2.252 | 2.250 | 2.250 | 2.250 | 2.254 | 2.250 | 2.241 | 2.247 |
| Octahedral | 2.086 | 2.087 | 2.092 | 2.075 | 2.082 | 2.084 | 2.081 | 2.087 | 2.083 | 2.092 | 2.088 | 2.077 | 2.138 | 2.107 |
| Interlayer | 3.333 | 3.319 | 3.316 | 3.331 | 3.323 | 3.314 | 3.336 | 3.308 | 3.326 | 3.323 | 3.326 | 3.320 | 3.339 | 3.310 |
| $D_{TM}$ (Å) | 0.453 | 0.459 | 0.449 | 0.497 | 0.470 | 0.469 | 0.484 | 0.463 | 0.480 | 0.464 | 0.478 | 0.493 | 0.451 | 0.452 |
| $\langle O\text{-}O\rangle_b$ (Å) | 2.634 | 2.638 | 2.635 | 2.652 | 2.642 | 2.644 | 2.649 | 2.645 | 2.659 | 2.646 | 2.654 | 2.654 | 2.673 | 2.652 |

*Notes*: α (tetrahedral rotation angle) = $\sum_{i=1}^{6} \alpha i / 6$ where $\alpha_i = |120° - \phi_i|/2$ and where $\phi_i$ is the angle between basal edges of neighboring tetrahedra articulated in the ring; Δz = [$z_{(Obasal)max}$ - $z_{(Obasal)min}$] [csinβ]; τ (tetrahedral flattening angle) = $\sum_{i=1}^{3} (Obasal - \hat{T} - Obasal)i / 3$; TAV (tetrahedral angle variance) = $\sum_{i=1}^{3} (\theta i - 109.47)^2 / 5$ (Robinson et al. 1971); TQE (tetrahedral quadratic elongation) = $\sum_{i=1}^{4} (l_i / l_o)^2 / 4$ where $l_o$ is the center to vertex distance for an undistorted tetrahedron whose volume is equal to that of the distorted tetrahedron with bond length $l_i$ (Robinson et al. 1971); ψ (octahedral flattening angle) = cos⁻¹[octahedral thickness / (2<M-O>)] (Donnay et al., 1964); OQE (octahedral quadratic elongation) $\sum_{i=1}^{6} (l_i / l_o)^2 / 6$ where $l_o$ is the center to vertex distance for an undistorted octahedron whose volume is equal to that of the distorted octahedron with bond length $l_i$ (Robinson et al., 1971); OAV (octahedral angle variance) = $\sum_{i=1}^{12} (\theta i - 90^\circ)^2 / 11$ (Robinson et al., 1971); $e_u$, $e_s$ (mean length of shared and unshared octahedral edges, respectively); $\Delta_{TM}$ (dimensional misfit) = $2\sqrt{3}$ <O-O>$_{basal}$ $-3\sqrt{2}$ (<M1-O> + <M2-O> + <M3-O>)/3 (Toraya, 1981). Labels (1), (2), a, and b as in Table 2.

**TABLE 6B.** Selected parameters derived from structure refinement for Li-poor crystals [layer symmetry *C*12/*m*(1)]

| Sample: | 26 | 33 | 120 |
|---|---|---|---|
| | **Tetrahedral parameters** | | |
| α (°) | 4.94 | 1.95 | 1.51 |
| Δz (Å) | 0.009 | 0.002 | 0.000 |
| τ (°) | 110.13 | 110.20 | 110.16 |
| TAV(°²) | 0.84 | 0.66 | 0.61 |
| TQE | 1.0007 | 1.0002 | 1.0002 |
| Volume (Å³) | 2.378 | 2.331 | 2.338 |
| | **Octahedral parameters** | | |
| $\psi_{M1}$ (°) | 58.97 | 58.55 | 58.76 |
| $\psi_{M2}$ (°) | 59.43 | 58.40 | 58.44 |
| $OQE_{M1}$ | 1.0118 | 1.0091 | 1.0102 |
| $OQE_{M2}$ | 1.0142 | 1.0086 | 1.0087 |
| $OAV_{M1}$ (°²) | 37.32 | 30.32 | 33.65 |
| $OAV_{M2}$ (°²) | 46.15 | 28.73 | 28.84 |
| $Volume_{M1}$ (Å³) | 11.450 | 12.334 | 12.458 |
| $Volume_{M2}$(Å³) | 11.870 | 12.185 | 12.143 |
| $e_u/e_s$ (M1) | 1.107 | 1.096 | 1.102 |
| $e_u/e_s$ (M2) | 1.119 | 1.092 | 1.088 |
| | **Sheet thickness (Å)** | | |
| Tetrahedral | 2.251 | 2.241 | 2.250 |
| Octahedral | 2.123 | 2.200 | 2.196 |
| Interlayer | 3.368 | 3.350 | 3.374 |
| $\Delta_{TM}$ (Å) | 0.392 | 0.394 | 0.402 |
| $\langle O\text{-}O\rangle_b$ (Å) | 2.689 | 2.689 | 2.693 |

*Notes*: α, Δz, t, TAV, TQE, ψ, OQE, OAV, $e_u$, $e_s$, and $\Delta_{TM}$ as in Table 6a.

$$Q_{M2,\,M3} = \frac{\left|\langle M3-O\rangle - \langle M2-O\rangle\right|}{\frac{1}{2}\left(\langle M3-O\rangle + \langle M2-O\rangle\right)}. \quad (3)$$

Additional information may be gleaned from the ordering parameter $E_{M2,\,M3}$ obtained by the mean electron count ($e^-$) at M2 and M3 sites:

$$E_{M2,M3} = \frac{\left|e^-M3 - e^-M2\right|}{\frac{1}{2}\left(e^-M3 + e^-M2\right)}. \quad (4)$$

The *C*12/*m*(1) to *C*12(1) symmetry transition is marked by the composition at which both $Q_{M2,M3}$ and $E_{M2,M3}$ go to zero. Actually, this point corresponds to the structural changes in which two symmetrically distinct sites become identical, leading to *C*12/*m*(1) symmetry of siderophyllite and annite.

Lithian micas from Pikes Peak appear to have a continuous range of composition spanning the ferroan polylithionite and siderophyllite fields and extending into the stability field of annite (Fig. 1). Because *C*12/*m*(1) layer symmetry was found for siderophyllite and annite, a progressive variation of $Q_{M2,\,M3}$ and $E_{M2,\,M3}$ as a function of $X_{Sid\text{-}Pl}$ should be expected. The values of $Q_{M2,\,M3}$ indicate that the transition from *C*12/*m*(1) to *C*12(1) symmetry starts approximately at $X_{Sid\text{-}Pl} \cong 0.6$, and that polylithionite and ferroan polylithionite crystals have virtually

**TABLE 7A.** Octahedral site cation distribution and mean electron counts for M1, M2, and M3 sites, and for unit cell ($e^-$) for Li-rich crystals [layer symmetry C12(1)]

| Sample: | 114 | 55a | 55b | 130(1) | 130(2) | 137 | 104 | 54b | 177 | 140(1) | 140(2) | 24 | 47 | 103 |
|---|---|---|---|---|---|---|---|---|---|---|---|---|---|---|
| | | | | | | | **M1** | | | | | | | |
| $Li^+$ | 0.615 | 0.412 | 0.531 | 0.558 | 0.531 | 0.362 | 0.345 | 0.391 | 0.438 | 0.369 | 0.332 | 0.200 | 0.138 | 0.308 |
| $Al^{3+}$ | 0.074 | 0.123 | 0.063 | 0.005 | 0.018 | 0.048 | 0.056 | 0.074 | – | 0.014 | – | 0.107 | 0.059 | 0.025 |
| $Fe^{2+}$ | 0.181 | 0.282 | 0.347 | 0.348 | 0.359 | 0.426 | 0.307 | 0.363 | 0.490 | 0.419 | 0.412 | 0.422 | 0.664 | 0.537 |
| $Fe^{3+}$ | 0.051 | 0.058 | 0.001 | 0.093 | 0.060 | 0.021 | 0.098 | – | – | 0.062 | 0.070 | 0.048 | 0.010 | – |
| $Mn^{2+}$ | 0.038 | – | – | – | – | – | – | – | – | – | – | – | 0.078 | 0.051 |
| □ | 0.049 | 0.136 | 0.066 | 0.006 | 0.037 | 0.146 | 0.198 | 0.178 | 0.075 | 0.139 | 0.185 | 0.229 | 0.065 | 0.083 |
| $e^-$ (calc.) | 9.79 | 11.68 | 11.46 | 13.20 | 12.72 | 13.33 | 12.29 | 11.57 | 14.05 | 13.80 | 13.53 | 14.21 | 20.66 | 16.49 |
| $e^-$ (X-ref) | 10.20 | 11.25 | 11.28 | 13.48 | 12.74 | 12.95 | 11.98 | 11.85 | 13.77 | 13.26 | 13.28 | 14.21 | 19.20 | 16.00 |
| $\langle M1\text{-}O\rangle_{calc.}$ | 2.121 | 2.124 | 2.126 | 2.130 | 2.123 | 2.127 | 2.130 | 2.133 | 2.130 | 2.132 | 2.132 | 2.129 | 2.144 | 2.132 |
| $\langle M1\text{-}O\rangle_{X\text{-}ref.}$ | 2.124 | 2.125 | 2.129 | 2.128 | 2.125 | 2.129 | 2.133 | 2.136 | 2.130 | 2.133 | 2.135 | 2.134 | 2.126 | 2.131 |
| | | | | | | | **M2** | | | | | | | |
| $Li^+$ | 0.777 | 0.012 | 0.001 | 0.001 | 0.002 | – | 0.025 | 0.042 | 0.110 | 0.001 | 0.024 | – | 0.080 | 0.002 |
| $Al^{3+}$ | – | 0.989 | 0.998 | 1.000 | 1.001 | 1.000 | 0.980 | 0.954 | 0.873 | 1.002 | 0.979 | 1.000 | 0.750 | 0.877 |
| $Fe^{2+}$ | 0.223 | – | – | – | – | – | – | – | – | – | – | – | – | – |
| $Fe^{3+}$ | – | – | – | – | – | – | – | – | – | – | – | – | 0.080 | 0.125 |
| $Ti^{4+}$ | – | – | – | – | – | – | – | – | 0.010 | – | – | – | 0.108 | – |
| □ | – | – | – | – | – | – | – | – | – | – | – | – | 0.005 | – |
| $e^-$ (calc.) | 8.13 | 12.89 | 12.98 | 13.00 | 13.02 | 13.00 | 12.82 | 12.53 | 11.90 | 13.03 | 12.80 | 13.00 | 14.45 | 14.66 |
| $e^-$ (X-ref) | 8.50 | 12.03 | 13.00 | 12.56 | 13.00 | 13.00 | 12.05 | 11.61 | 12.73 | 13.00 | 12.43 | 12.34 | 15.80 | 14.30 |
| $\langle M2\text{-}O\rangle_{calc.}$ | 2.115 | 1.890 | 1.883 | 1.887 | 1.891 | 1.885 | 1.900 | 1.887 | 1.899 | 1.891 | 1.896 | 1.885 | 1.983 | 1.915 |
| $\langle M2\text{-}O\rangle_{X\text{-}ref.}$ | 2.122 | 1.888 | 1.882 | 1.890 | 1.890 | 1.885 | 1.890 | 1.883 | 1.891 | 1.891 | 1.896 | 1.885 | 2.017 | 1.916 |
| | | | | | | | **M3** | | | | | | | |
| $Li^+$ | 0.031 | 0.706 | 0.690 | 0.522 | 0.562 | 0.611 | 0.598 | 0.518 | 0.314 | 0.484 | 0.496 | 0.564 | 0.207 | 0.313 |
| $Al^{3+}$ | 0.966 | – | – | – | – | – | – | – | – | – | – | – | – | – |
| $Mg^{2+}$ | – | 0.008 | 0.005 | 0.022 | 0.021 | 0.011 | 0.012 | 0.008 | 0.009 | 0.051 | 0.052 | 0.003 | 0.054 | 0.022 |
| $Fe^{2+}$ | – | 0.249 | 0.198 | 0.354 | 0.352 | 0.247 | 0.331 | 0.246 | 0.157 | 0.387 | 0.391 | 0.356 | 0.729 | 0.652 |
| $Fe^{3+}$ | – | – | 0.062 | – | 0.003 | 0.054 | 0.052 | 0.122 | 0.240 | – | 0.006 | 0.002 | 0.006 | – |
| $Mn^{2+}$ | – | 0.038 | 0.045 | 0.062 | 0.062 | 0.073 | 0.010 | 0.063 | 0.064 | 0.058 | 0.060 | 0.079 | – | – |
| □ | – | – | 0.004 | 0.040 | 0.001 | 0.010 | 0.003 | 0.047 | 0.214 | 0.023 | – | – | – | 0.020 |
| $e^-$ (calc.) | 12.65 | 9.64 | 10.02 | 12.58 | 12.72 | 11.62 | 12.15 | 12.79 | 12.97 | 13.58 | 13.93 | 13.01 | 20.38 | 18.16 |
| $e^-$ (X-ref) | 12.20 | 9.38 | 9.90 | 12.76 | 12.74 | 11.28 | 11.84 | 12.96 | 12.84 | 13.00 | 13.73 | 12.97 | 19.40 | 17.64 |
| $\langle M3\text{-}O\rangle_{calc.}$ | 1.887 | 2.120 | 2.124 | 2.124 | 2.121 | 2.131 | 2.125 | 2.127 | 2.129 | 2.127 | 2.128 | 2.129 | 2.103 | 2.131 |
| $\langle M3\text{-}O\rangle_{X\text{-}ref.}$ | 1.885 | 2.124 | 2.127 | 2.127 | 2.125 | 2.131 | 2.123 | 2.132 | 2.131 | 2.129 | 2.131 | 2.133 | 2.085 | 2.129 |
| $\Sigma e^-_{2(M1+M2+M3)calc.}$ | 61.1 | 68.4 | 68.9 | 77.6 | 76.9 | 75.9 | 74.5 | 73.8 | 77.9 | 80.8 | 80.5 | 80.4 | 111.0 | 98.6 |
| $\Sigma e^-_{2(M1+M2+M3)X\text{-}ref}$ | 61.8 | 65.3 | 68.4 | 77.6 | 77.0 | 74.5 | 71.7 | 72.8 | 78.6 | 78.5 | 78.9 | 79.0 | 109.0 | 95.9 |
| $\Sigma e^-_{(M1+M2+M3)EPMA}$ | 61.4 | 68.7 | 69.5 | 78.0 | 77.2 | 76.5 | 74.8 | 74.4 | 78.7 | 81.5 | 81.2 | 80.6 | 111.3 | 99.4 |

*Note*: Labels (1), (2), a, and b as in Table 2. Values were obtained after the octahedral site distribution ($Se^-_{2(M1+M2+M3)calc}$), by structure refinement ($Se^-_{2(M1+M2+M3)X\text{-}ref}$), and by electron microprobe analysis ($Se^-_{(M1+M2+M3)EMPA}$).

the same degree of octahedral ordering (Fig. 4a). In contrast, with decreasing M2 and M3 metrical deviation, the $E_{M2,M3}$ parameter indicates an increase in ordering (see samples 103 and 47, Fig. 4b). These observations suggest that: (1) there is a difference in a crystal chemical response of the octahedral sites to $X_{Sid\text{-}Pl}$; (2) The order-disorder transition occurs in a narrow compositional interval; (3) during the order-disorder transition, M3 site grows richer in iron and controls the distribution of octahedral cations (Tables 7a and 7b).

From the listing of M site occupancies, the projected ratios of Li/(Li+$Fe^{2+}$) on cis-M1 site [$X_{Li}$(cis)] and trans-M2 (or -M3) sites [$X_{Li}$(trans)] show a small but consistent preference on the part of Li for trans-sites (Fig. 5). In *C*12(1) crystals, the mean intracrystalline partition coefficient between M1 and M3 sites [$(Li/Fe)_{M1}/(Li/Fe)_{M3}$) = 0.67 ± 0.07], shows no consistent detectable changes with M2 occupancy, which appears to change only when the layer approaches *C*12/*m* (1) symmetry. This establishes a consistent preference of $R^{3+}$ cations for M2 and indicates that both M1 and M3 sites are sensitive to changes in composition along the join. The octahedra sites M3 (M2 in sample 114) and M1 show the largest angular deviation from a perfect octahedron and M2 (M3 in sample 114) has the smallest, as measured by octahedral angle variance parameter (OAV) and octahedral flattening angle (ψ) (Table 6a). As $X_{Sid\text{-}Pl}$ increases, so does the angular distortion of M1 and M3, by contrast with M2, in which the angular distortion decreases (Tables 6a and 6b).

**TABLE 7B.** Octahedral site cation distribution and mean electron counts for M1 and M2 sites, and for unit cell ($e^-$) for Li-poor crystals [layer symmetry *C*12/*m*(1)]

| | $M_1$ | | | M2 = M3 | | |
|---|---|---|---|---|---|---|
| | 26 | 33 | 120 | 26 | 33 | 120 |
| $Li^+$ | 0.170 | 0.083 | – | – | – | – |
| $Al^{3+}$ | 0.203 | – | – | 0.318 | 0.176 | 0.066 |
| $Mg^{2+}$ | 0.100 | – | 0.107 | – | – | – |
| $Fe^{2+}$ | 0.507 | 0.824 | 0.894 | 0.563 | 0.698 | 0.703 |
| $Fe^{3+}$ | – | – | – | 0.124 | 0.080 | 0.107 |
| $Mn^{2+}$ | 0.017 | 0.078 | – | – | – | – |
| $Ti^{4+}$ | – | – | – | 0.015 | 0.056 | 0.126 |
| □ | – | 0.010 | 0.001 | 0.004 | 0.002 | 0.002 |
| $e^-$ (calc.) | 17.96 | 23.62 | 24.53 | 22.33 | 23.75 | 24.69 |
| $e^-$ (X-ref) | 19.55 | 23.48 | 24.74 | 22.32 | 23.87 | 24.43 |
| $<M\text{-}O>_{calc.}$ | 2.059* | 2.110* | 2.114* | 2.084† | 2.096† | 2.096† |
| $<M\text{-}O>_{X\text{-}ref.}$ | 2.059* | 2.109* | 2.117* | 2.087† | 2.100† | 2.098† |
| $\Sigma e^-_{2(M1+2M2)calc.}$ | 125.2 | 142.2 | 147.8 | | | |
| $\Sigma e^-_{2(M1+2M2)X\text{-}ref}$ | 128.4 | 142.4 | 147.2 | | | |
| $\Sigma e^-_{(M1+2M2)EPMA}$ | 123.9 | 142.1 | 147.3 | | | |

*Notes:* Values obtained after the octahedral site distribution ($\Sigma e^-_{2(M1+2M2)calc}$), by structure refinement ($\Sigma e^-_{2(M1+2M2)X\text{-}ref}$), and by electron microprobe analysis ($\Sigma e^-_{(M1+2M2)EPMA}$).
* M = M1
† M = M2 = M3

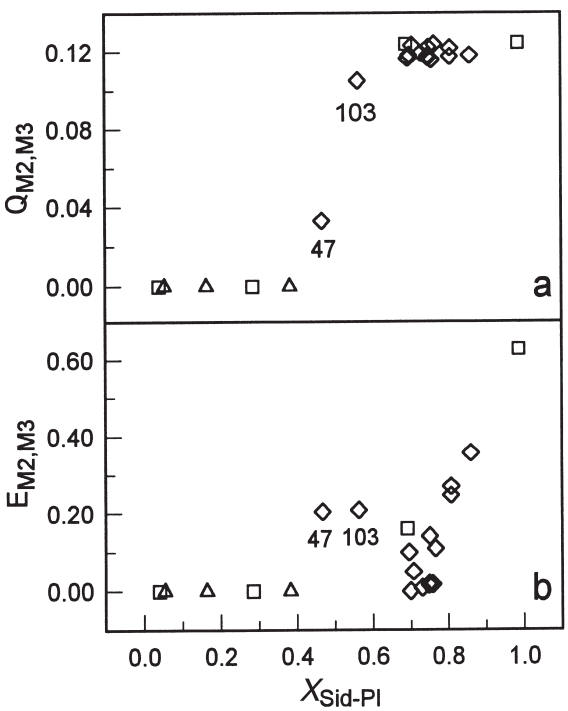


**FIGURE 4.** Variation of (**a**) $Q_{M2,M3}$ (Eq. 3) and (**b**) $E_{M2,M3}$ (Eq. 4) parameters as a function of composition. The data points at $Q_{M2,M3}$ and $E_{M2,M3}$ = 0 correspond to *C*12/*m*(1) crystals. Symbols and samples as in Figure 3. The number 47 and 103 refer to lithian siderophyllite crystal 47 and 103, respectively.

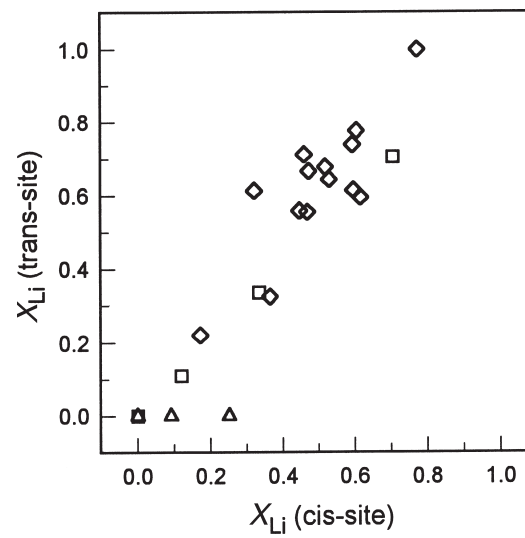


**FIGURE 5.** Plot of $X_{Li}$ [$X_{Li}$ = Li/(Li + Fe)] in cis-M3 (or -M2) site vs. $X_{Li}$ in trans-M1 site. Symbols and samples as in Figure 3.

The different composition and degree of ordering of octahedral sites creates differences in bond valence arrangement on O3, O33, and O4 sites (Guggenheim 1981). Because O3 and O33 atoms are the bridging atoms of the tetrahedra, it is expected that differences in the octahedral features may affect the configuration of the tetrahedral sheet.

The tetrahedral mean bond lengths of the T1 and T11 tetrahedra ⟨T1-O⟩ and ⟨T11-O⟩ correlate well with $X_{Sid\text{-}Pl}$, ⟨T1-O⟩ ranging from 1.632 to 1.658 Å and ⟨T11-O⟩ from 1.635 to 1.643

Å. Comparison of the individual T-O bond lengths shows that the increase in ⟨T1-O⟩ depends on the increase in each T1-O distance, whereas ⟨T11-O⟩ variation, although very small, primarily results from differences in the T11-O33 distance (Table 5a). Both tetrahedra show similar distortion, as measured by the tetrahedral quadratic elongation (TQE), and tetrahedral flattening (t), and they become more distorted as $X_{Sid-Pl}$ increase (Tables 6a and 6b; Figs. 6a and 6b). The correlation between $^{[4]}$Al ($0.928 \leq {}^{[4]}\text{Al} \leq 2.115$ apfu, mean value: $1.505 \pm 0.007$ apfu) from microprobe analysis (Table 2) and ⟨T1-O⟩ ($1.632 \leq \langle T1\text{-}O \rangle \leq 1.658$ Å, mean value: $1.643 \pm 0.002$ Å) (Fig. 6b) shows a small, but consistent, preference of Al for T1 site rather than for the T11 site. Consistency in partitioning of $Al^{3+}$ in the T1 site is confirmed in lithian siderophyllite (sample 47), where the difference between T1 and T11 mean bond lengths was estimated to be 0.021 Å (standard deviation of the mean value, $s_n$ = 0.003 Å). As pointed out by Guggenheim (1981) the apical O3 anion is more closely coordinated to the Al-rich M2 site than is the apical O33 anion of the T11 tetrahedron. The Al concentration in T1 would cause the apical O3 atom to be undersaturated and favor the presence of a highly charged cation in M2. Also, the different octahedral ordering pattern in ferroan polylithionite (sample 114) would be a consequence of the bond valence compensation on O33 atom: even though not statistically significant, T11 is slightly larger than T1 and accounts for Al substitution in the former.

Two more parameters, the out-of-plane tilting of the tetrahedral basal oxygen (Δz) and the tetrahedral rotation (α) describe the way in which the tetrahedral sheet accomplished changes in M site composition and degree of ordering. Tetrahedral rotation, which reduces the lateral dimensions of the tetrahedral sheet to provide a good fit with octahedra by O3 and O33 atoms, is generally small ($1.5 \leq \alpha \leq 5.0°$) and roughly increases with $X_{Sid-Pl}$, with no noticeable differences related to cation ordering. The Δz parameter, produced by tetrahedral tilting around octahedra, is remarkably sensitive both to $X_{Sid-Pl}$ and to the degree of octahedral order. According to Lee and Guggenheim (1981), high Δz values are produced by the unequal shape and dimensions of octahedral sites. Table 6 shows that lithian siderophyllite (samples 103 and 47), which approach *C*12*/m*(1) layer symmetry, siderophyllite and annite crystals display the lowest Δz values, whereas ferroan polylithionite display the highest. Therefore the reduced differences in the M2 and M3 site volumes with decreasing $X_{Sid-Pl}$ require less tetrahedral tilting to fit O3 and O33 atoms.

In *C*12(1) crystals, the reduction of O4-O4 and M2-O4 bond lengths due to F in O4 and Al in M2 sites would cause the O4 anion to be oversaturated and would favor the increase in the A-O4 distance. The interlayer cation would be propped up in the cavity and would link more closely to the basal O2, O22 and O1 atoms, thereby reducing the A-O inner distances and creating a concomitant increase in interlayer separation (Table 6a).

In summary, this study demonstates that: (1) Li- Fe-bearing micas present a complex octahedral order-disorder pattern; (2) in *C*12(1) crystals, $Al^{3+}$ is strongly ordered on one of the octahedral cis-sites, whereas Li and Fe are disordered on the remaining positions with a slight preference of Li for M3; (3) only when the siderophyllite content approaches the end-member M2 and M3 become equivalent; (4) the unit-cell parameters *a* and *b* are affected by the whole octahedral composition, whereas c decreases with $^{[6]}$Al and, therefore, is sensitive to the relative dimension of cis-octahedra.

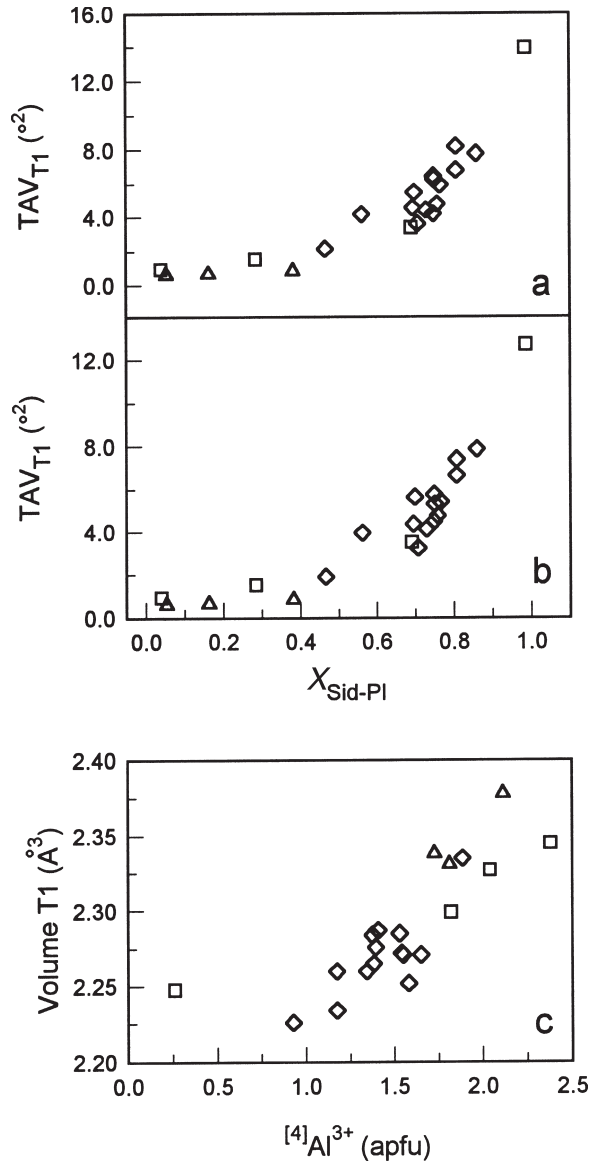


**FIGURE 6.** Variation of tetrahedral angle variance for (**a**) T1 and T11 (**b**) as a function of composition. (**c**) Variation of T1 volume in lithium-bearing micas as a function of $^{[4]}$Al determined by electron microprobe. Symbols and samples as in Figure 3.

## ACKNOWLEDGMENTS

The authors thank the Italian MURST (project "Layer silicates: crystal chemical, structural, and petrological aspects") for financial support, and the CIGS (Modena and Reggio Emilia University) for their help and advice during the course of this study. The manuscript was reviewed by D. Eberl (U.S. Geological Survey), E. Galli (University of Modena and Reggio Emilia), P.J. Modreski (U.S. Geological Survey), M. Nespolo (Tokyo University), and M. Rieder (Charles University, Praha).

## REFERENCES CITED


Backhaus, K.O. (1983) Structure refinement of a lepidolite-1M. Crystal Research Technology, 18, 1253–1260.

Brigatti, M.F. and Davoli, P. (1990) Crystal-structure refinements of 1M plutonic biotites. American Mineralogist, 75, 305–313.

Brigatti, M.F., Frigieri, P., and Poppi, L. (1998) Crystal chemistry of Mg-, Fe-bearing muscovites-$2M_1$. American Mineralogist, 83, 775–785.

Brown, B.E. (1978) The crystal structure of a 3*T* lepidolite. American Mineralogist, 63, 332–336.

Busing, W.R., Martin, K.O., and Levy, H.A. (1962) ORFLS, a Fortran crystallographic least-squares refinement program. U.S. National Technical Information Service, ORNL-TM-305.

Carpenter, M.A., Domeneghetti, M.C., and Tazzoli, V. (1990) Application of Landau theory to cation ordering in omphacite. I: Equilibrium behaviour. European Journal of Mineralogy, 2, 7–18.

Černý, P. (1991) Rare-element granitic pegmatites, part I. Anatomy and internal evolution of pegmatite deposits. Geosciences Canada, 18, 49–67.

Creagh, D.C. and McAuley, W.J. (1995) X-ray dispersion correction. In A.J.C. Wilson, Ed., International Tables for Crystallography, Volume C, p. 206–219. Kluwer Academic Publishers, Dordrecht, Holland.

Dornberger-Schiff, K., Backhaus, K.O., and Ďurovič, S. (1982) Polytypism of micas:OD-interpretation, stacking symbols, symmetry relations. Clays and Clay Minerals, 30, 364–374.

Ďurovič, S. (1994) Classification of phyllosilicates according to the symmetry of their octahedral sheet. Silikáty, 38, 81–84.

Ďurovič, S., Weiss, Z., and Backhaus, K.O. (1984) Polytypism of micas. II Classification and abundance of MDO polytypes. Clays and Clay Minerals, 32, 464–474.

Donnay, G., Morimoto, N., Takeda, H., and Donnay, J.D.H. (1964) Trioctahedral one-layer micas: I. Crystal structure of a synthetic iron mica. Acta Crystallographica, 17, 1369–1373.

Donovan, J.J. (1995) PROBE: PC-based data acquisition and processing for electron microprobes. Advanced Microbeam, 4217 C King Graves Rd., Vienna, Ohio, 44473.

Foley, S.F. (1989) Experimental constraints on phlogopite chemistry in lamproites: 1. The effect of water activity and oxygen fugacity. European Journal of Mineralogy, 1, 411–426.

Foord, E.E., Černý, P., Jackson, L.L., Sherman, D.M., and Eby, R.K. (1995) Mineralogical and geochemical evolution of micas from miarolitic pegmatites of the anorogenic Pikes Peak batholith, Colorado. Mineralogy and Petrology, 55, 1–26.

Gottesmann, B. and Tischendorf, G. (1978) Klassifikation, chemismus und optik trioktaedrischer glimmer. Zeitschrift für Geologische Wissenschaften, Berlin, 6, 681–708.

Guggenheim, S. (1981) Cation ordering in lepidolite. American Mineralogist, 66, 1221–1232.

Guggenheim, S. and Bailey S.W. (1977) The refinement of zinnwaldite-1M in subgroup symmetry. American Mineralogist, 62, 1158–1167.

Hazen, R.M. and Burnham, C.W. (1973) The crystal structures of one-layer phlogopite and annite. American Mineralogist, 58, 889–900.

Kile, D.E. and Foord, E.E. (1998) Micas from the Pikes Peak batholith and its cogenetic granitic pegmatites, Colorado: optical properties, composition, and correlation with pegmatite evolution. Canadian Mineralogist, 36, 463–482.

Lee, J.H. and Guggenheim, S. (1981) Single crystal X-ray refinement of pyrophyllite-1*Tc*. American Mineralogist, 66, 350–357.

Maslen, E.N., Fox, A.G., and O'Keefe, M.A. (1995) X-ray scattering. In A.J.C. Wilson, Ed., International Tables for Crystallography, Volume C, p. 476–509. Kluwer Academic Publishers, Dordrecht, Holland.

Meyrowitz, R. (1970) New semi-micro-procedure for determination of ferrous iron in refractory silicate minerals using a sodium metafluoborate decomposition. Analytical Chemistry, 42, 1110–1113.

Moler, C. (1992) The student edition of MATLAB, 495 p. The Math Works Inc., Prentice Hall, Englewood Cliff, New York.

Munoz, J.L. (1984) F-OH and Cl-OH exchange in micas with applications to hydrothermal ore deposits. In Mineralogical Society of America Reviews in Mineralogy, 13, 469–493.

Nespolo, M., Takeda, H., Kogure, T., and Ferraris, G. (1999) Periodic intensity distribution (PID) of mica polytypes: symbolism, structural model orientation and axial settings. Acta Crystallographica, A55, 659–676.

Rieder, M., Pichová, A., Fassová, M., Fediuková, E., and Černý, P. (1971) Chemical composition and physical properties of lithium-iron micas from Krušné hory (Erzebirge), Czechoslovakia and Germany. Part B: Cell parameters and optical data. Mineralogical Magazine, 38, 190–196.

Rieder, M., Cavazzini, G., D'Yakonov, Y., Frank-Kamenetskii, V.A., Gottardi, G., Guggenheim, S., Koval, P.V., Müller, G., Neiva, A.M.R., Radoslovich, E.W., Robert, J.-L., Sassi, F.P., Takeda, H., Weiss, Z., and Wones, D.R. (1998) Nomenclature of the micas. The Canadian Mineralogist, 36, 905–912.

Rieder, M., Hybler, J., Smrčok, L., and Weiss, Z. (1996) Refinement of the crystal structure of zinnwaldite $2M_1$. European Journal of Mineralogy, 8, 1241–1248.

Robinson, K., Gibbs, G.V., and Ribbe, P.H. (1971) Quadratic elongation: a quantitative measure of distortion in coordination polyhedra. Science, 172, 567–570.

Sartori, F. (1976) The crystal structure of a 1M lepidolite. TMPM Tschermaks Mineralogische und Petrographische Mitteilungen, 23, 65–75.

———(1977) Crystal structure of a $2M_1$ lepidolite. TMPM Tschermaks Mineralogische und Petrographische Mitteilungen, 24, 23–37.

Sartori, F., Franzini, M., and Merlino, S. (1973) Crystal structure of a $2M_2$ lepidolite. Acta Crystallographica, B29, 573–578.

Sheldrick, G.M. (1993) SHELX-93, program for crystal structure determination. University of Göttingen, Germany.

Siemens (1996) XSCANS: X-ray single crystal analysis system—Technical reference. Siemens instruments. Madison, Wisconsin, U.S.A.

Simmons, W.B., Lee, M.T., and Brewster, R.H. (1987) Geochemistry and evolution of the South Platte granite-pegmatite system, Jefferson County, Colorado. Geochimica and Cosmochimica Acta, 51, 455–471.

Swanson, T.H. and Bailey, S.W. (1981) Redermination of the lepidolite-$2M_1$ structure. Clays and Clay Minerals, 29, 81–90.

Takeda, H. and Burnham, C.W. (1969) Fluor-polylithionite: a lithium mica with nearly hexagonal $(Si_2O_5)^{2-}$ ring. Mineralogical Journal, 6, 102–109.

Takeda, H., Haga, N., and Sadanaga, R. (1971) Structural investigation of a polymorphic transition between $2M_2$-, 1M-lepidolite and $2M_1$-muscovite. Mineralogical Journal, 6, 203–215.

Toraya, H. (1981) Distorsions of octahedral and octahedral sheets in 1M micas and the relation to their stability. Zeitschrift für Kristallographie, 157, 173–190.

Unruh, D.M., Snee, L.W., Foord, E.E., and Simmons, W.B. (1995) Age and cooling history of the Pikes Peak batholith and associated pegmatites. Geological Society of America Abstracts with Programs, 27, A-468.

Weiss, Z., Rieder, M., Chmielová, M., and Krajíček, J. (1985) Geometry of octahedral coordination in micas: a review of refined structures. American Mineralogist, 70, 747–757.

Weiss, Z., Rieder, M., Smrčok, L., Petříček, V., and Bailey, S.W. (1993) Refinement of the crystal structures of two "protolithionites". European Journal of Mineralogy, 5, 493–502.

Wobus, R.A. and Hutchinson, R.M. (1988) Proterozoic plutons and pegmatites of the Pikes Peak region, Colorado. In G.S. Holden, Ed., Field trip guidebook: Professional Contribution no. 12, p. 35–42. GSA 1888–1988 Centennial Meeting, Colorado School of Mines, Denver.

Zvyagin, B.B. (1997) Modular analysis of crystal structures. EMU notes in Mineralogy, S. Merlino Ed., Eötvös University Press, 345–371.


MANUSCRIPT RECEIVED JULY 13, 1999
MANUSCRIPT ACCEPTED MARCH 10, 2000
PAPER HANDLED BY JEFFREY E. POST